Supporting Information

Moraga-Cid et al. 10.1073/pnas.1417864112

SI Materials and Methods

Protein Production. The cDNA coding for Lily-His consists, from the N to the C terminus, of a *Drosophila* signal peptide (MKLCILLAVVAFVGLSLG), the mature sequence of Lily followed to a C-terminal his-tag inserted into a pMT/BiP/V5-HisA vector (Invitrogen). This plasmid and the pPURO selection plasmid (19 μg and 1 μg, respectively) were cotransfected into S2-type insect cells in the presence of cellfectin (Invitrogen). Cotransfected cell lines were grown in Insect-XPRESS medium (Lonza) supplemented with 0.6 μg/mL puromycine at 28 °C without CO_2. Cell lines are considered stable after 3–4 wk. Protein expression is induced upon addition of cadmium (5 μM) when the culture reaches a cell-density population of 10^7 cells/mL. Cells were collected by centrifugation (1,500 × *g* for 10 min). Lily-His was extracted and purified following the same procedure as described previously (1). In brief, cells were broken by sonication at 4 °C in buffer A (20 mM Tris, 300 mM NaCl). Membranes were recovered by centrifugation (1 h at 186,000 × *g*) and solubilized using 2% DDM in buffer A with agitation overnight at 4 °C. The supernatant was collected by centrifugation at 46,500 × *g* (1 h). Lily was finally recovered from the supernatant by affinity chromatography using Cobalt resin, eluted using imidazole (250 mM), and purified by size exclusion chromatography.

Crystallography.

Crystal preparation. All crystals were obtained using vapor diffusion in hanging drops at 20 °C. The concentrated (6–8 mg/mL) protein was mixed in a 1:1 ratio with reservoir solution typically containing 16–20% PEG 2000MME, 50 mM $NiCl_2$, 4% DMSO, 11% ethylene glycol, and 0.1 M NaAcetate, pH 3.0. Crystallization was induced by the microseeding technique from a solution of crushed crystals 1 h after setting up the crystallization experiment. Crystals appeared overnight and grew for 1 wk before reaching their final dimensions (typically 100 μm × 100 μm × 100 μm). All crystals were cryoprotected, using a three-step protocol: (*i*) The crystal-containing drops were transferred to the cold room (4 °C), sealed onto a novel crystal plate that contained no reservoir solution, and left at 4 °C for 10 min; (*ii*) 3–5 μL of a dehydrating solution composed of the reservoir solution supplemented with 30% of ethylene glycol was added to the crystallization drop; and (*iii*) the drop was left to air dry for 5–20 min before flash freezing in liquid nitrogen.

Data collection. Datasets were collected on beamline ID23-1 of the European Synchrotron Radiation Facility (Grenoble, France). Crystals were collected using the helicoidal data collection facility. Reflections were integrated using XDS (2) and further processed using the CCP4 programs (2). Crystals of Lily-His belong to the $P2_12_12_1$ space group (*a*, *b*, *c* = 118.9 Å, 132.3 Å, and 190.5 Å and α = β = γ = 90°) with one pentamer in the asymmetric unit. Details on the data collection statistics are provided in Table S1.

Phasing and refinement. The molecular replacement solution was found in Phaser (3) by using the structure of GLIC (PDB ID: 4HFI) at 2.4 Å as a starting model. This initial model was refined in Refmac 5 (4) by using rigid-body refinement and subsequently by using restrained refinement (4). The resulting model was improved by manual building in COOT (5). The model was finally refined in Buster (6). Automatically generated noncrystallographic symmetry restraints were thus used throughout refinement (7). Right after molecular replacement, B factors were reset to an arbitrary value of 120 corresponding to the Wilson-plot estimated B factors and set constant until the final steps of refinement. B factors were then refined using two translation/libration/screw (TLS) groups by chain [one for the ECD (residues 5–191) and one for the TMD (residues 218–413)]. NCS symmetry averaging improves the quality of the electron density, thus allowing the unambiguous reconstruction of the main chain except for the first four N-terminal residues and the M1–M2 loop (residues 218–222) as well as the C-terminal 10-histidine expression tag. For model geometry validation, 94.8% of the residues were in the most favored regions of the Ramachandran plot. MolProbity scores (8) for the refined model ranged within the 100th percentiles of structures refined at comparable resolutions. Details of the refinement statistics are provided in Table S1.

Homology Modeling. We constructed three homology models of Lily. The first model completes the missing parts of the crystal structure of Lily-His in the LC state. The others propose a model of Lily in the open state (based on GLIC-pH4) and the resting state (based on GLIC-pH7). We manually created the sequence alignment between GLIC and Lily, as it is straightforward because only one gap could be found in the M1–M2 loop.

For the LC structural model of Lily, we used as a template the presented crystal structure of Lily as well as parts of the crystal structure of GLIC in the same crystal packing (see below). The homology models were constructed while keeping all completely attributed residues, in the used Lily structure, as rigid body constraints, and thus not modified. To model the missing part of the M1–M2 loop we used the structure of four residues of GLIC in the M1–M2 loop [residues 218–221 (STST), ST–SY, Fig. 1] as a structural template. For the last of the five Lily chains, the last helix turn of M1 was missing, and we used the same strategy as described previously, by adding residues 213–216 (TAFW) from GLIC as a structural template. For the open model of Lily, we used as a template the high-resolution structure of GLIC in the open state (PDB ID: 4HFI) (9). The whole ECD (residues 5–191) of GLIC was used as a rigid body constraint with the exception of the two loops in contact with the TMD, loop 2 (residues 31–33) and loop 7 (residues 112–122).

The Modeler software (10) was used to generate 100 homology models of each state. The best-scoring model was chosen for the last step of side-chain refinement. All residue side chains that were not part of the rigid body restraints were rebuilt using the backbone-dependent rotamer library SCRWL4 (11). Radii were calculated using the program Hole (12).

Electrophysiology.

cDNA constructs. The cDNA construct encoding the Lily receptors with a C-terminal HA-tag subcloned into the pMT3 vector for expression in BHK cells has been described previously (13). Mutations were inserted by using the QuikChange site-directed mutagenesis method. All constructions were confirmed by full sequencing.

Cell culture and transfection. BHK cells, tk-ts13 variant, display weak endogenous proton-gated currents and are therefore favorable to record Lily and its mutants. Cells were grown at 37 °C under a 5% CO_2 atmosphere in DMEM with Glutamax (Invitrogen), supplemented with 5% FBS (FBS), penicillin (0.1 g/L), and streptomycin (100 units/mL). Cells were seeded at 104 cells/cm^2 in 35-mm Petri dishes 24 h before transfection. Cells were transfected with 4 μg of cDNA of interest and 1 μg of GFP-cDNA cloned into the pMT3 vector, using the calcium phosphate precipitation method, and GFP-positive cells were used for electrophysiology 16–24 h after transfection. For recordings performed

in S2 cells, stable cell lines were grown in Insect-XPRESS medium supplemented with 0.6 μg/mL puromycine at 28 °C without CO_2. Five days before patch experiments, Lily expression was induced upon addition of cadmium (5 μM). One day before, cells were plated in 35-mm dishes coated with poly-L-lysine (Sigma-Aldrich).

Patch-clamp recordings. Whole-cell recordings in BHK and S2 cells were performed using a holding potential of −60 mV. Patch electrodes were filled with 140 mM CsCl, 2 mM $MgCl_2$, 2 mM Ca_2Cl, 10 mM BAPTA, and 10 mM Hepes (pH 7.4). The external solution contained 150 mM NaCl, 10 mM KCl, 2.0 mM $CaCl_2$, 1.0 mM $MgCl_2$, 10 mM Hepes (pH 7.4), and 10 mM glucose. The amplitude of currents was assayed using a brief (1–2 s) pulse with external solution at the desired pHs every 60 s. Proton dose–response curves were calculated, normalizing the maximal current at each proton concentration to the maximal current obtained at saturating concentrations of the protons (100%). EC_{50}, nH, and τ_{act} values and plots were constructed using the Origin 6.0 (MicroCal) software. To calculate the coupling energy between pairs of residues, mutant cycle analysis was performed as described previously (14) using the equation

$$\Delta G = RT \ln \left[\frac{EC_{50,\,ww} \times EC_{50,\,mm}}{EC_{50,\,wm} \times EC_{50,\,mw}} \right],$$

where ΔG is the coupling energy, R is the universal gas constant, T is temperature (K), $EC_{50,ww}$ is the wild-type EC_{50} value, $EC_{50,mm}$ is the double-mutant EC_{50} value, and $EC_{50,mw}$ and $EC_{50,wm}$ are the two single-mutant EC_{50} values.

The methodology for single-channel recordings in the outside-out configuration has been previously published (13). Briefly, patch pipettes had tip resistances of 7–15 Mohm following fire polishing. Patches were voltage clamped at −60 mV and the data were filtered (5-kHz low-pass eight-pole Bessel) and acquired at 50 kHz, using pClamp software (Molecular Devices). The solutions at different pHs were applied to the patch, using a gravity-driven solution exchanger perfusion system. Cells were maintained in extracellular medium containing 150 mM NaCl, 10 mM KCl, 2.0 mM $CaCl_2$, 1.0 mM $MgCl_2$, 10 mM Hepes (pH 7.4), and 10 mM glucose. The intracellular recording solution contained 140 mM CsCl, 2 mM $MgCl_2$, 2 mM Ca_2Cl, 10 mM BAPTA, and 10 mM Hepes (pH 7.4). Conductance values were obtained from plots I/V constructed using the Origin 6.0 software.

1. Bocquet N, et al. (2009) X-ray structure of a pentameric ligand-gated ion channel in an apparently open conformation. *Nature* 457(7225):111–114.
2. Collaborative Computational Project, Number 4 (1994) The CCP4 suite: Programs for protein crystallography. *Acta Crystallogr D Biol Crystallogr* 50(Pt 5):760–763.
3. McCoy AJ, et al. (2007) Phaser crystallographic software. *J Appl Cryst* 40(Pt 4):658–674.
4. Murshudov GN, Vagin AA, Dodson EJ (1997) Refinement of macromolecular structures by the maximum-likelihood method. *Acta Crystallogr D Biol Crystallogr* 53(Pt 3): 240–255.
5. Emsley P, Cowtan K (2004) Coot: Model-building tools for molecular graphics. *Acta Crystallogr D Biol Crystallogr* 60(Pt 12 Pt 1):2126–2132.
6. Blanc E, Roversi P, Vonrhein C, Flensburg C, Lea SM, et al. (2004) Refinement of severely incomplete structures with maximum likelihood in BUSTER-TNT. *Acta Crystallogr D Biol Crystallogr* 60(Pt 12 Pt 1):2210–2221.
7. Smart OS, et al. (2012) Exploiting structure similarity in refinement: Automated NCS and target-structure restraints in BUSTER. *Acta Crystallogr D Biol Crystallogr* 68(Pt 4): 368–380.
8. Davis IW, Leaver-Fay A, Chen VB, Block JN, Kapral GJ, et al. (2007) MolProbity: All-atom contacts and structure validation for proteins and nucleic acids. *Nucleic Acids Res* 35(Web Server issue):W375–383.
9. Sauguet L, et al. (2014) Crystal structures of a pentameric ligand-gated ion channel provide a mechanism for activation. *Proc Natl Acad Sci USA* 111(3):966–971.
10. Sali A, Blundell TL (1993) Comparative protein modelling by satisfaction of spatial restraints. *J Mol Biol* 234(3):779–815.
11. Krivov GG, Shapovalov MV, Dunbrack RL, Jr (2009) Improved prediction of protein side-chain conformations with SCWRL4. *Proteins* 77(4):778–795.
12. Smart OS, Goodfellow JM, Wallace BA (1993) The pore dimensions of gramicidin A. *Biophys J* 65(6):2455–2460.
13. Duret G, et al. (2011) Functional prokaryotic-eukaryotic chimera from the pentameric ligand-gated ion channel family. *Proc Natl Acad Sci USA* 108(29):12143–12148.
14. Bode A, Lynch JW (2013) Analysis of hyperekplexia mutations identifies transmembrane domain rearrangements that mediate glycine receptor activation. *J Biol Chem* 288(47):33760–33771.

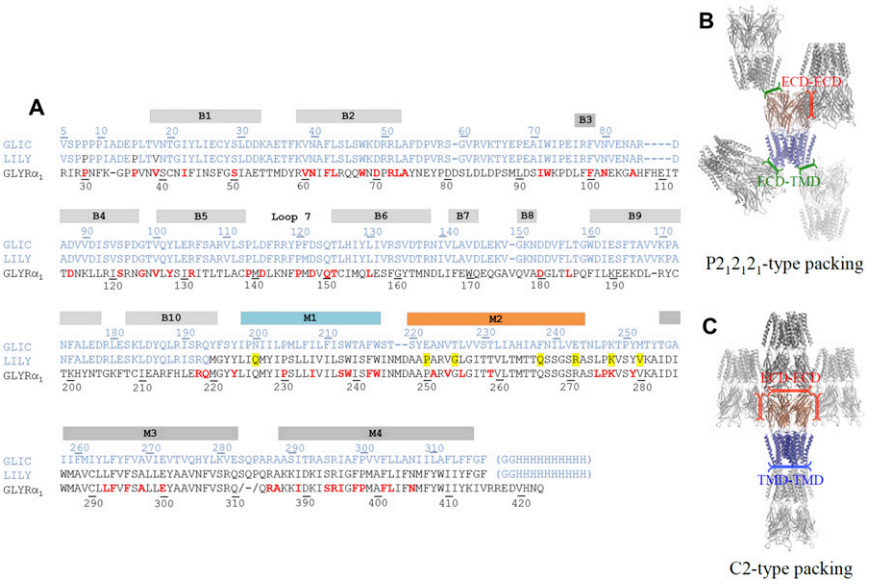

Fig. S1. Crystal packing of Lily. (*A*) Sequence alignment between GLIC (blue), Lily (blue and black), and α_1GlyR (black). Conserved residues are indicated in red and the mutated residues in Lily are indicated in yellow. (*B* and *C*) P222 crystal packing of Lily (*B*) and comparison with the C2 packing obtained for GLIC-pH4 (*C*).

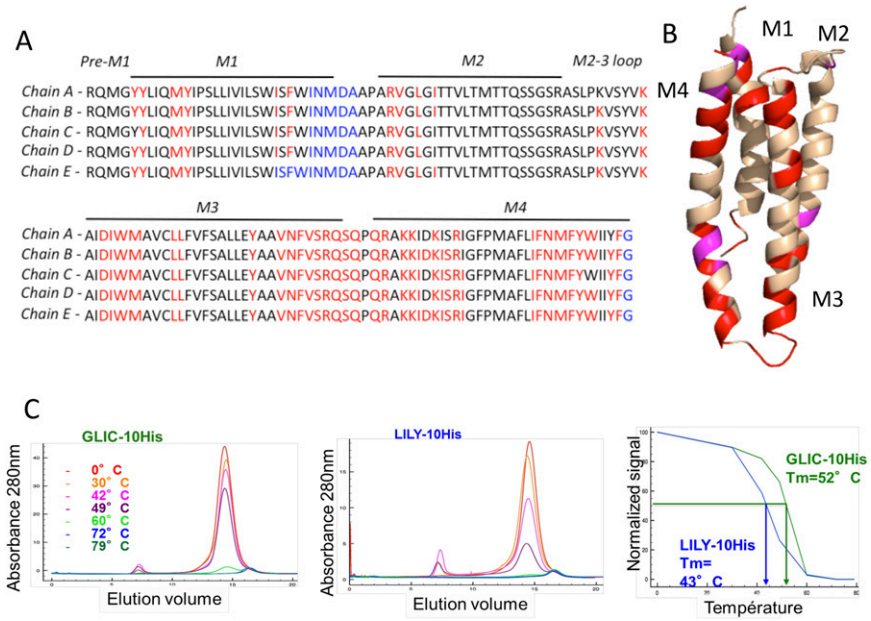

Fig. S2. Missing atoms in the Lily refined crystal structure. (*A*) Sequence alignment of the five chains constituting the TMD of Lily. Residues are respectively colored in blue or red when the whole residue or its side chain has been omitted from the final model. (*B*) Cartoon representation of a TMD of Lily. Residues are colored in red when their side chains are missing in all five monomers and in pink when modeled in at least one monomer. (*C*) Thermostability of GLIC-His and Lily purified in detergent solution. The purified protein samples (500 μL at 0.2 mg/mL) were incubated over a range of temperatures for 10 min, using a thermal cycler, followed by centrifugation to remove precipitated material. The supernatant was then loaded onto a superose 6 column equilibrated with SEC buffer [20 mM Tris (pH 7.5), 300 mM NaCl, 0.02% DDM] and run at the flow rate of 0.5 mL/min. The eluent was detected by UV absorption at 280 nm. Lily thus displays marked flexibility at the level of M4 and at the cytoplasmic side of the TMD, a feature observed in the crystal and possibly related to the lower thermal stability of Lily vs. GLIC observed in detergent solution. Such flexibility may have several origins: (*i*) It may be due to the lack of the intracellular domain, an ∼88-aa segment between M3 and M4 that is present in α_1GlyR but has been removed in Lily (however, it is noteworthy that in the GluCl structures, the bottom segment of the TMD is well ordered whereas the cytoplasmic domain was removed in a similar manner to that in Lily); (*ii*) specific lipids may be needed to constrain the TMD of the α_1GlyR, a feature well documented for nAChRs; and (*iii*) an interesting possibility would be that the α_1GlyR carries a TMD intrinsically flexible in its closed-channel conformation. This may be related to its TMD structure that carries a single ring of hydrophobic residues at position 261 that hold together the M2 helices in the closed channel, together with the presence of two rings of glycine residues at positions 254 and 256 that may confer backbone flexibility. Thus, the observed flexibility might be an intrinsic property of the closed-channel conformation, a feature that might have functional implications for channel activation. Upon activation, a conformational change might stabilize the intracellular side of the TMD as well as the intracellular end of the pore that hosts the selectivity filter.

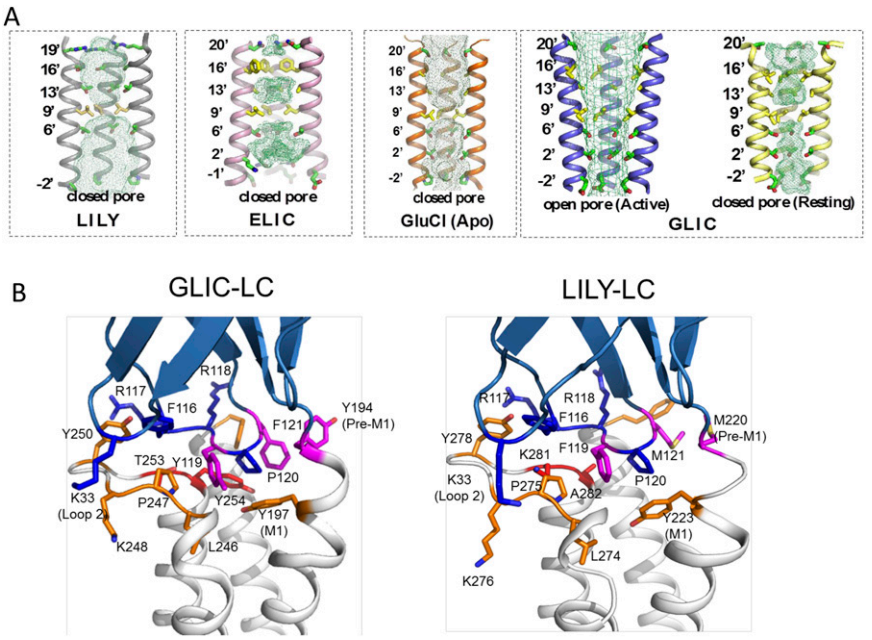

Fig. S3. (*A*) Ion permeation pathway. Shown are cartoon representations of the ion channel of Lily, ELIC (PDB ID: 2VL0), GLIC active (PDB ID: 4HFI), GLIC resting (PDB ID: 4NPQ), and GluCl Apo (PDB ID: 4TNV), with the two front helices removed. The green grids show the volume accessible to the solvent. Side chains of pore-lining residues are shown as sticks. (*B*) ECD–TMD interface in Lily and GLIC-LC. Shown is a cartoon representation of the domain interface of a monomer of GLIC-LC and Lily with the ECD colored blue and the TMD colored white. Residues contributing to the interface are shown as sticks and colored according to their location and conservation between GLIC and Lily. At the ECD, conserved (vs. nonconserved) residues are colored blue (vs. magenta). At the TMD conserved (vs. nonconserved) residues are colored orange (vs. red).

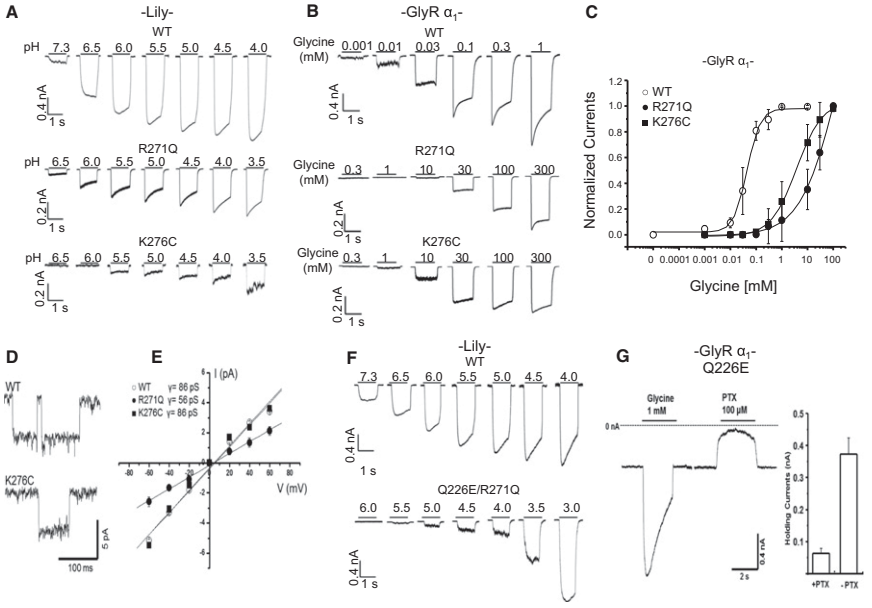

Fig. S4. Electrophysiological characterization of Lily and α_1GlyR mutants. (*A*) Typical current traces of whole-cell recordings for Lily WT and R271Q and K276C mutants. (*B*) Typical current traces of whole-cell recordings for the α_1GlyR (without tag) WT and R271Q and K276C mutants. (*C*) Normalized dose–response curves for α_1GlyR WT and the indicated mutants. (*D*) Single-channel events recording at −60 mV and pH 6.0 of outside-out patches containing Lily WT or K276C mutant. (*E*) The I/V relationship plots summarized the mean channel amplitude obtained at different voltages of Lily WT and R271Q and K276C mutants. (*F*) Typical current traces of whole-cell recordings for Lily WT and Q226E/R271Q double mutant. (*G*) Sample trace for α_1GlyR Q226E mutant showing the leak current observed without glycine, the maximal glycine-elicited current (1 mM), and the inhibition of the leak current by 100 μM picrotoxin (PTX) (quantified in the bar graph where error bars represent ±SD).

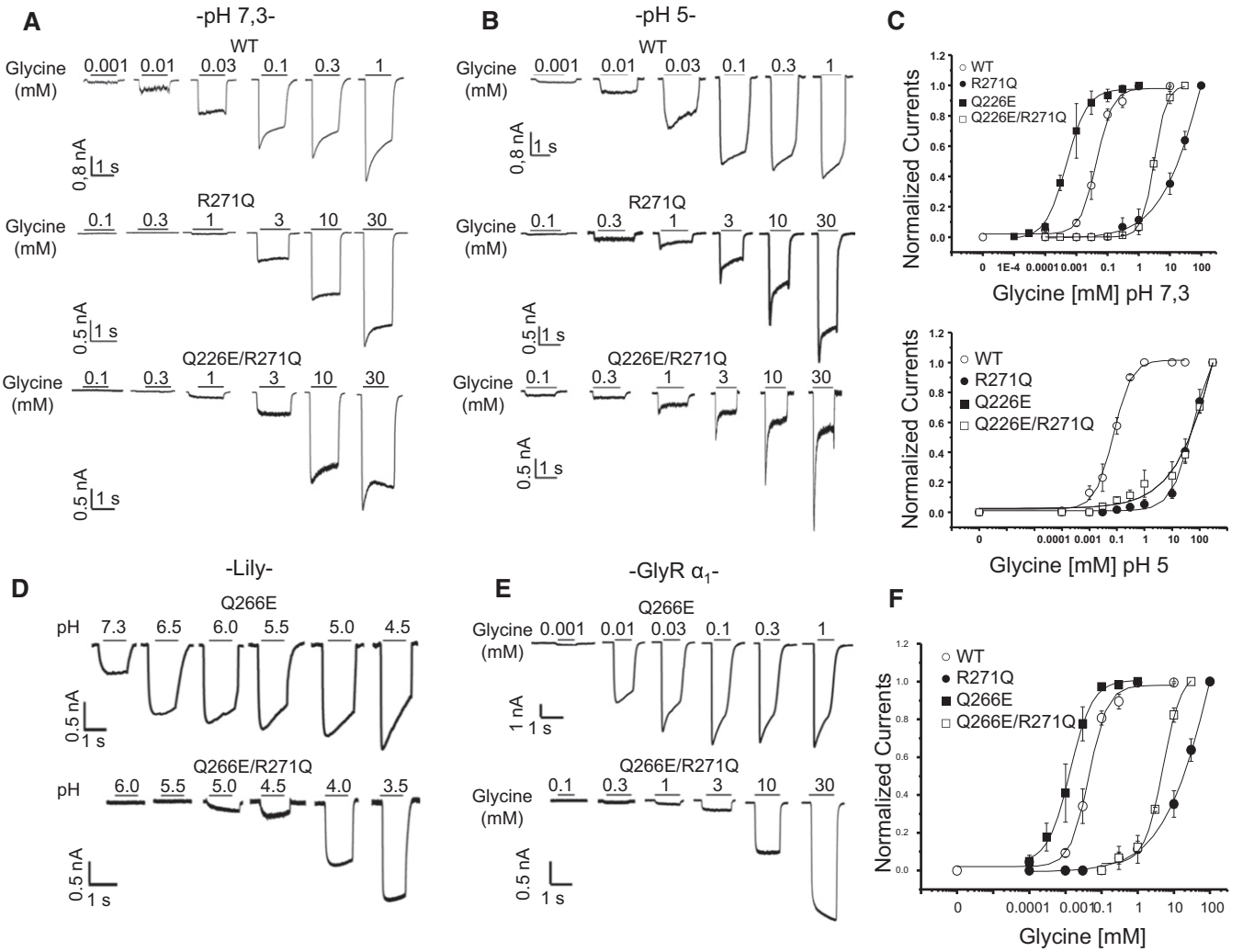

Fig. S5. Electrophysiological characterization of Lily and α1GlyR mutants. (*A*) Typical current traces of whole-cell recordings for α_1GlyR WT and R271Q and Q226E/R271Q mutants performed at pH 7.3. (*B*) Typical current traces of whole-cell recordings for α_1GlyR WT and R271Q and Q226E/R271Q mutants performed at pH 5. BHK cells were maintained in bath solution at pH 7.3 and glycine application (0.01–30 mM) was performed at pH 5. Note that the change in pH profoundly changes the pattern of activation by protons for mutants R271Q and Q226E/R271Q. At pH 7.3, glycine dose–response curves are well fitted by the Hill equation, whereas at pH 5 dose–responses curves seem to contain two components: a "high-affinity component" underlying weak activation at a low concentration of glycine and a "low-affinity component" underlying strong activation at a high concentration of glycine. In addition, pH seems to alter the shape of the currents. (*C*) (*Upper*) Normalized dose–response curves for α_1GlyR WT (EC_{50} 44 ± 6 μM), R271Q (EC_{50} 20 ± 2.5 mM), and Q226E/R271Q (EC_{50} 3.1 ± 0.4 mM) recorded at pH 7.3. (*Lower*) Normalized dose–response curves for α_1GlyR WT (EC_{50} 78 ± 7μM), R271Q (EC_{50} 57 ± 8 mM), and Q226E/R271Q (EC_{50} 49 ± 6 mM) recorded at pH 5. (*D*) Typical current traces of whole-cell recordings for Lily WT and Q266E and Q266E/R271Q mutants. (*E*) Typical current traces of whole-cell recordings for α_1GlyR WT and Q266E and Q266E/R271Q mutants. (*F*) Normalized dose–response curves for α_1GlyR WT and the indicated mutants.

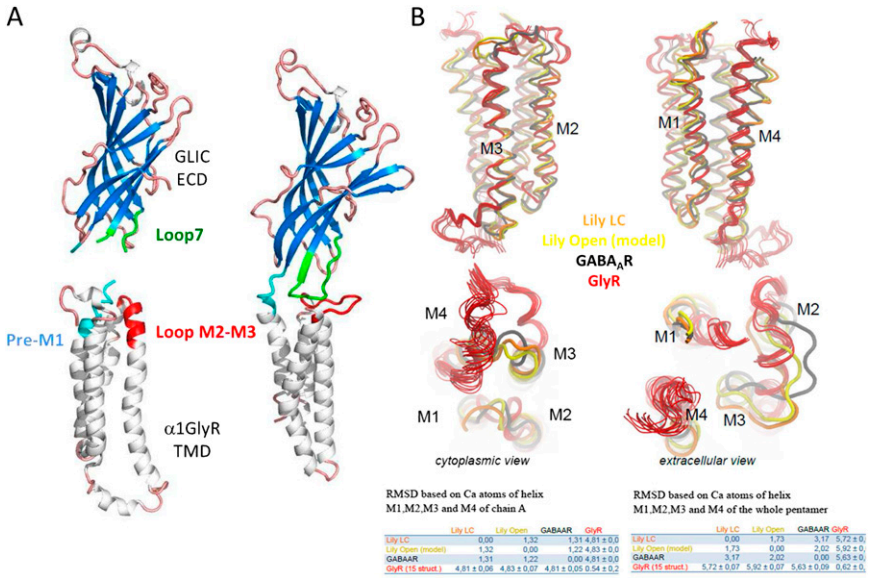

Fig. S6. (*A*) Modular structure of Lily. Shown is a cartoon representation of the X-ray structure of Lily, of GLIC-ECD expressed alone, and of the TMD of the α_1GlyR expressed alone and solved by NMR. The β-strands of the ECD are colored blue, the α-helices of the TMD are colored white, and the loops pink. Loop 7, pre-M1, and loops M2–M3 are colored respectively green, cyan, and red. (*B*) Comparison of the TMDs of Lily and GABA$_A$ X-ray structures with the α_1GlyR NMR models. The TMDs of Lily, the Lily open model, the GABA$_A$R model (PDB ID: 4COF) (1), and the α_1GlyR NMR model (PDB ID: 2M6I) (2) are represented as orange, yellow, black, and red tubes, respectively. Note that α_1GlyR structure has been solved using NMR, and as a consequence 15 structures have been displayed. All structures have been aligned using Cα atom coordinates of M1, M2, M3, and M4 helices and M2–M3 loop. (*Right*) The rsmd of all presented structure vs. themselves. Two atom selections have been used for this calculation; the first selection contains the first of the five chains of Cα atoms coordinates of the four helices, and the second selection contains the five chains of Cα atoms coordinates of the four helices. These models show marked differences between the α_1GlyR NMR models and the Lily TMD structure. Differences in the M3–M4 loop at the bottom are probably due to a different linker, which is longer in the isolated TMD (REFGGGGFI sequence) than in Lily (SQP sequence). However, the rest of the TMD is identical in sequence between both structures, and we observed marked differences in the relative orientations of the helices. In addition, the M2–M3 linker is partly folded in the helix and highly dynamic in the NMR models whereas it is folded in an extended conformation in Lily. The secondary structure of the TMD is highly conserved in all X-ray structures solved so far. It is highly unlikely that the TMD of the α_1GlyR would fold in a different manner. The difference of the isolated TMD structure may be due to (*i*) a lack of structural constraints applied by the ECD; (*ii*) a mobilizing effect of the micellar environment (3); and (*iii*) the fact that the NMR data may be compatible with other structural models because, in particular, the set of Overhauser effect (NOE) connectivity and paramagnetic relaxation enhancement (PRE) restraints cannot be unambiguously assigned to inter- or intrasubunit distances, and the initial model used to build the TMD was based on residual dipolar coupling (RDC) constraints on a peptide comprising only the M2 and M3 segments (4).

1. Mowrey DD, et al. (2013) Open-channel structures of the human glycine receptor α1 full-length transmembrane domain. *Structure* 21(10):1897–1904.
2. Miller PS, Aricescu AR (2014) Crystal structure of a human GABAA receptor. *Nature* 512(7514):270–275.
3. Bond PJ, Sansom MS (2003) Membrane protein dynamics versus environment: Simulations of OmpA in a micelle and in a bilayer. *J Mol Biol* 329(5):1035–1053.
4. Canlas CG, Ma D, Tang P, Xu Y (2008) Residual dipolar coupling measurements of transmembrane proteins using aligned low-q bicelles and high-resolution magic angle spinning NMR spectroscopy. *J Am Chem Soc* 130(40):13294–13300.

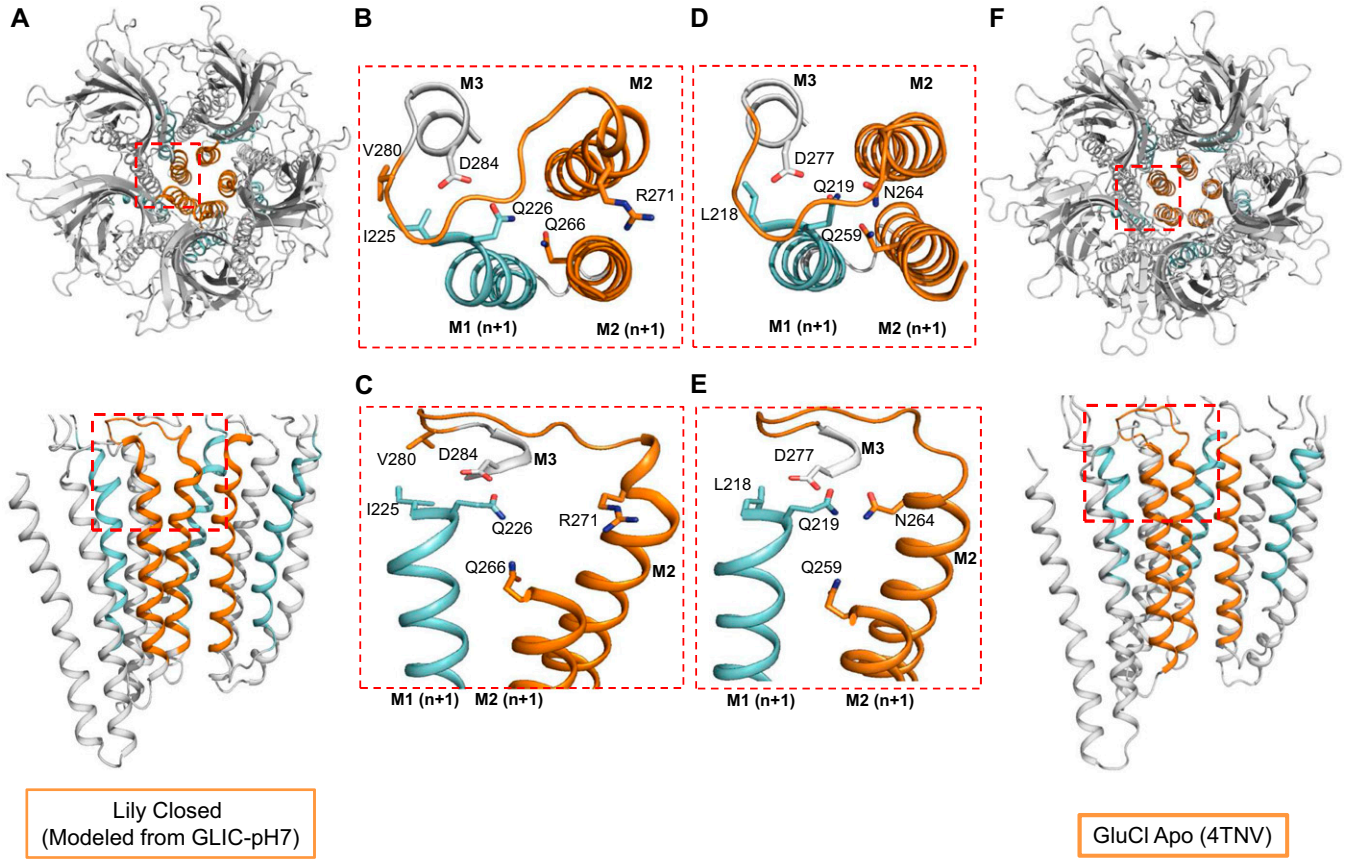

Fig. S7. Closed-channel conformation of Lily (modeled by homology using GLIC-pH7) (PDB ID: 4NPQ) and comparison with the GluCl-apo closed (4TNV) structure. Views of Lily (*A* and *B*) and GluCl (*E* and *H*) are represented in the same manner as in Fig. 6 *B* and *E*. M2 of a single subunit is colored orange and the neighboring M1 and M2 from the adjacent subunit are colored cyan and pale orange, respectively. (*C* and *F*) Side views of Lily (*C*) and GluCl (*F*). Side chains of Q226, Q266, R271, and D284 residues in Lily (*E*) and the homologous Q219, N259, N264, and D277 in GluCl (*F*) are shown as sticks.

Table S1. Data collection and refinement statistics

Data collection	
Space group	$P2_12_12_1$
Cell dimensions	
a, *b*, *c*, Å	118.9, 132.3, 190.5
α, β, γ, °	90, 90, 90
Resolution, Å	49.4–3.50 (3.68–3.50)
R_{pim}	0.036 (0.638)
R_{merge}	0.065 (1.12)
$I/\sigma(I)$	12.8 (1.2)
Resolution at which $I/\sigma(I) = 2$	3.65
Completeness, %	99.8 (99.9)
Redundancy	4.9 (5.0)
Refinement	
Resolution, Å	25.0–3.50
No. reflections	38,364
R_{work}/R_{free}	25.4/27.1
No. atoms	
Protein	11,407
Ligand/ion	9
B factors	
Protein	174.3
Ligand/ion	168.9
Molprobity analysis	
Ramachandran favored, %	94.8
Ramachandran outliers, %	0.46
Molbrobity score[†]	100th
rms deviations	
Bond lengths, Å	0.007
Bond angles, °	0.92

[†]One hundredth percentile is the best among structures of comparable resolution; 0th is the worst.

Table S2. Properties of Lily and GlyR wild-type and mutant receptors

	Lily						GlyR					
Receptor	EC_{50}, M $[H^+]$	EC_{50} Mut/ EC_{50} WT	I_{max}, nA	nH	Conduct, pS	*n*	EC_{50}, M [glycine]	EC_{50} Mut/ EC_{50} WT	I_{max}, nA	nH	Conduct, pS	*n*
WT	$2.6 \pm 0.5 \times 10^{-7}$	1	1.6 ± 0.31	1.2 ± 0.2	86 ± 2	14	$44 \pm 2 \times 10^{-6}$	1	2.26 ± 0.31	1.7 ± 0.2	90 ± 3	10
Q226E	ND	—	1.2 ± 0.25	—	85 ± 2	6	$4.7 \pm 0.2 \times 10^{-6}$	0.1	1.66 ± 0.3	1.3 ± 0.2	—	6
P250T	$1.2 \pm 0.2 \times 10^{-5}$	46	0.3 ± 0.12	1.3 ± 0.2	—	6	$570 \pm 80 \times 10^{-6}$	13	0.8 ± 0.12	1.3 ± 0.2	—	6
G254A	$2.6 \pm 0.2 \times 10^{-7}$	1	1.3 ± 0.31	1.2 ± 0.4	126 ± 3	7	$42 \pm 3 \times 10^{-6}$	1	2.1 ± 0.31	1.1 ± 0.4	—	5
Q266E	$8.7 \pm 0.3 \times 10^{-8}$	0.3	1.1 ± 0.28	1.2 ± 0.2	—	6	$14 \pm 2 \times 10^{-6}$	0.3	6.66 ± 0.8	1.4 ± 0.2	—	5
R271Q	$2.8 \pm 0.5 \times 10^{-6}$	10	1.1 ± 0.31	1.3 ± 0.4	56 ± 3	7	$20 \pm 2.5 \times 10^{-3}$*	454	0.98 ± 0.27	1.2 ± 0.4	—	5
K276C	$3.1 \pm 0.2 \times 10^{-5}$*	119	0.2 ± 0.11	1.1 ± 0.4	87 ± 3	7	$3.8 \pm 0.9 \times 10^{-3}$*	86	1.7 ± 0.11	1.3 ± 0.4	—	6
V280M	ND	—	—	—	86 ± 3	5	NP	—	—	—	—	—
Q226E/R271Q	$1.5 \pm 0.2 \times 10^{-4}$*	576	0.6 ± 0.35	1.2 ± 0.2	—	4	$3.1 \pm 0.4 \times 10^{-3}$*	70	2.1 ± 0.3	2.2 ± 0.3	—	5
Q266E/R271Q	$6.07 \pm 0.3\ 10^{-5}$	233	0.7 ± 0.29	1.1 ± 0.3	—	5	$4.9 \pm 0.6 \times 10^{-3}$*	112	1.96 ± 0.3	1.6 ± 0.2	—	5

*For these mutants, the plateau response of the dose–response curves could not be accurately achieved. ND, not determined; NP, not performed. All error values are given as ±SD.